Histol Histopathol (2008) 23: 1229-1240

http://www.hh.um.es

Histology and Histopathology

Cellular and Molecular Biology

The histopathology of a human mesenchymal stem cell experimental tumor model: support for an hMSC origin for Ewing's sarcoma?

Jorge S. Burns[1], Basem M. Abdallah[1], Henrik D. Schrøder[2] and Moustapha Kassem[1]

[1]Department of Endocrinology and Metabolism and [2]Institute of Pathology, Odense University Hospital, Odense, Denmark

Summary. Sarcomas display varied degrees of karyotypic abnormality, vascularity and mesenchymal differentiation. We have reported that a strain of telomerized adult human bone marrow mesenchymal stem cells (hMSC-TERT20) spontaneously evolved a tumorigenic phenotype after long-term continuous culture. We asked to what extent our hMSC-TERT20 derived tumors reflected events found in human sarcomas using routine histopathological procedures. Early versus late passage hMSC-TERT20 cultures persistently expressed mesenchymal lineage proteins e.g. CD105, CD44, CD99 and vimentin. However, late passage cultures, showed increased immuno-histochemical staining for CyclinD1 and p21WAF1/Cip1, whereas p27Kip1 staining was reduced. Notably, spectral karyotyping showed that tumorigenic hMSC-TERT20 cells retained a normal diploid karyotype, with no detectable chromosome abnormalities. Consistent with the bone-forming potential of early passage hMSC-TERT20 cells, tumors derived from late passage cells expressed early biomarkers of osteogenesis. However, hMSC-TERT20 cells were heterogeneous for alpha smooth muscle actin (ASMA) expression and one out of six hMSC-TERT20 derived single cell clones was strongly ASMA positive. Tumors from this $ASMA^+$ clone had distinctive vascular qualities with hot spots of high $CD34^+$ murine endothelial cell density, together with CD34- regions with a branching periodic acid Schiff reaction pattern. Such clone-specific differences in host vascular response provide novel models to explore interactions between mesenchymal stem and endothelial cells. Despite the lack of a characteristic chromosomal translocation, the histomorphology, biomarkers and oncogenic changes were similar to those prevalent for Ewing's sarcomas. The phenotype and ontogenesis of hMSC-TERT20 tumors was consistent with the hypothesis that sarcomas may arise from hMSC, providing a unique diploid model for exploring human sarcoma biology.

Key words: Adult bone marrow stem cells, Cancer stem cells, Cell culture, Angiogenesis

Offprint requests to: Jorge S. Burns, PhD, Laboratory for Molecular Endocrinology, KMEB, Department of Endocrinology and Metabolism, Odense University Hospital, Medical Biotechnology Center, Winsløwparken 25.1, DK-5000 Odense C, Denmark. e-mail: jburns@health.sdu.dk

Introduction

Though relatively rare (less than 5% of adult or 20% of pediatric neoplasms), soft tissue sarcomas pose a significant diagnostic dilemma and are proportionally more malignant in the young. Osteogenic sarcoma and Ewing's sarcoma have peak incidence in childhood and young adults, whereas chondrosarcomas principally occur in people over 65 years old (Clark et al., 2005). Most sarcomas are sporadic and etiology is poorly understood, although there are four known familial cancer syndromes, including a higher incidence of osteosarcoma in patients with germline mutations of the retinoblastoma (RB) gene (Hansen et al., 1985). Broadly, sarcomas can be categorized as those with near-diploid karyotypes and specific reciprocal translocations, or those with complex karyotypes, no reproducible translocation patterns and p53 alterations. A confounding factor in sarcoma diagnosis is unknown histogenesis and wide histological diversity. This can range from poor differentiation, to features resembling normal connective tissue elements such as bone, cartilage, fat and muscle; the presumed tissues of origin. A poor prognosis, unchanged in the last 20 years,

beckons alternatives to traditional radiotherapy to improve therapeutic efficacy (Weitz et al., 2003). The response to radiotherapy is most likely to be governed by the tumor cell's intrinsic radiosensitivity, but it has been proposed that the apoptotic response of the surrounding microvascular cells may also be significant (Garcia-Barros et al., 2003). Despite significant improvements with chemotherapy, the rate of survival for aggressive sarcomas like advanced Ewing's sarcoma remains little more than 55% (Grier et al., 2003). In the quest for novel therapies, there is growing interest in suggestions that cancer cells may exhibit stem cell-like properties (Crowe et al., 2004; Bjerkvig et al., 2005) and that the development of the vasculature essential to tumor growth may have non-conventional mechanisms beyond angiogenesis, such as vasculogenic mimicry (Folberg and Maniotis, 2004) or vasculogenesis involving endothelial progenitor cells (Bagley et al., 2005).

Here, we extend previous studies concerning immortalization of primary bone marrow-derived human mesenchymal stromal cells using retroviral vector mediated expression of the human telomerase reverse transcriptase gene (hMSC-TERT) (Simonsen et al., 2002). Though early passage strains retained an excellent osteogenic and adipogenic differentiation potential (Abdallah et al., 2005), a late passage strain, hMSC-TERT20, passaged at a lower seeding density, evolved a clonable tumorigenic phenotype (Serakinci et al., 2004; Burns et al., 2005). Given potential implications for expansion of therapeutic stem cells, we wished to determine whether tumorigenic change might be forseen by screening for mesenchymal biomarker expression, oncological markers or karyotypic stability. Therefore, we immunohistochemically compared chronologically early (non-tumorigenic) versus late (tumorigenic) passage cultures and determined their karyotype. Furthermore, asking to what extent our tumors derived from the hMSC-TERT20 strain and its clones might usefully mimic human sarcoma biology, we analysed tissue-specific lineage markers and a range of oncological prognostic markers. Given different tumor growth rates for hMSC-TERT20 clones in our earlier studies, we examined angiogenesis for each clone. Murine-specific endothelial cell staining quantified by Chalkley counts and Periodic acid Schiff reaction staining revealed clonal heterogeneity with regard to the host vasculature response. Such differences in angioarchitecture have implications for delivery of anti-tumor therapeutic agents and how stem cells qualities might influence host vasculature when adult mesenchymal stem cells are used as therapeutic agents in ischaemic situations (Kinnaird et al., 2004).

Materials and methods

Cell culture

The hMSC-TERT20 strain and its derived clones, designated hMSC-TERT20-BB3, -BC8, -BD6, -BD11, -CE8 and -DB9 were grown in phenol red-free MEM (Gibco Invitrogen Co., Tastrup, Denmark) supplemented with 10% fetal bovine serum (FBS; Gibco Invitrogen Co., batch tested) and antibiotics Penicillin/Streptomycin (Gibco Invitrogen Co.) as described (Burns et al., 2005). For multicellular spheroid cultures, 10^6 cells were seeded on ultra-low adhesion tissue culture dishes (Corning, Biotech Line A/S, Slangerup, Denmark) and incubated overnight at 37°C in a 5% CO_2 humidified incubator (Hereus).

Flourescent activated cell sorting (FACS) cytometry

Cells harvested using trypsin with 0.1% EDTA (Invitrogen) were centrifuged at 200xg for 5 min at 4°C. Cell pellets resuspended in ice-cold phosphate buffered saline (PBS^{--}) were fixed with ice-cold 96% ethanol. The nuclei were released and the RNA removed using a 0.04% pepsin solution (Sigma) in 0.1M HCl and subsequently treated with 10 μg/ml RNase (Qiagen) in PBS-TB (PBS + 0.5% (v/v) Tween-20 (Merck) + 0.1% (w/v) BSA). Nuclei were spun down and resuspended in 50 μg/ml Propidium Iodide (PI) (Sigma) in PBS-TB and incubated overnight at 4°C. Samples were filtered on a 50 μm nylon mesh and flow cytometric measurements were performed on 10,000-20,000 cells using a FACScan™ flow cytophotometer (Becton Dickinson); argon laser (488-nm excitation and >695 nm fluorescence emission).

Karyotypic analysis

For metaphase spreads, cells fed 10-12 h previously were treated with 0.02 μg/mL colcemid (Karyomax, Gibco BRL) 3-4 h before harvesting. Cell pellets washed in PBS were resuspended in 5 mL 0.056 M KCl hypotonic buffer for 30 min at room temperature before pelleting the cells at 160xg for 10 min. Cells resuspended in 1mL hypotonic buffer were fixed in methanol:glacial acetic acid (3:1 v/v), washed in fixative, then released as single drops onto a glass slide from a height of 10 cm. G-band cytogenetics was performed using standard procedures (Yunis, 1976), analyzing at least 25 mitoses. Spectral karyotyping (SKY) to refine cytogenetic diagnosis was performed as described (Schrock et al., 1997). Pretreatment, denaturing and hybridization of the 24 chromosome-specific painting probes followed the manufacturer's instructions (Applied spectral imaging, Migdal HaEmek, Israel). Each sample consisted of at least ten fully analyzed mitoses.

Total RNA extraction and Real-Time-PCR

Total RNA was isolated from cultured cells with TRIzol® (Invitrogen A/S, Tastrup, Denmark) according to the manufacturer's instructions. Real-time PCR procedures were as described (Abdallah et al., 2005).

For target gene VEGF-A, forward primer 5'-CTACCTCCACCATGCCAAGTG-3' and reverse primer 5'-TGATTCTGCCCTCCTCCTTCT-3' yielded a 62 bp product. For normalising gene ß-actin, forward primer 5'-TGTGCCCATCTACGAGGGGTATGC-3' and reverse primer 5'-GGTACATGGTGGTGCCGCC AGACA-3' yielded a 430 bp product. Fold induction and expression levels were calculated using the comparative Ct method (formula [1/(2ΔCt)], where ΔCt is the difference between Ct target gene and Ct-reference) normalized to ß-actin mRNA (PerkinElmer's User Bulletin No. 2). Data analysis used the optical system software v3.0 (Bio Rad) and Microsoft Excel 2000.

Immunohistochemistry

Routinely used diagnostic and/or prognostic indicators in the Odense University Hospital Pathology department were examined (Table 1). Detection employed immunoperoxidase and Envision Plus according to the manufacturer's instructions (Dako, Glostrup, Denmark). For lineage analysis of hMSC-TERT 20 tumors (n=10) and tumors derived from its clones, deparaffinised 4 μm thick sections were tested immunohistochemically for antigens characteristic of different tissues: Smooth muscle; alpha smooth muscle actin (ASMA), calponin: Muscle; desmin, myogenin: Bone; biglycan, osteonectin, bone sialoprotein (BSP), procollagen type1 nitrogenous propeptides (P1NP), collagen type Ia,: Schwann cells; S100: Neuronal cells; CD56: Endothelial cells; CD31, CD34: Haematopoietic bone marrow cells; CD45: Basement lamina; laminin, collagen type IV: Epithelium; cytokeratin (CAM5,2) (Table 2).

In vivo tumorigenicity and bone formation assay

Prior protocols were performed for tumorigenicity (Burns et al., 2005) and bone formation assays (Abdallah et al., 2005). For the latter, hMSC-TERT20 cells in medium were mixed with hydroxyapatite/tricalcium phosphate (HA/TCP) (Zimmer Scandinavia, Broendby, Denmark), incubated overnight at 37°C and implanted subcutaneously under the dorsal surface of 8-week-old female NOD/LtSz-Prkdcscid mice. Implants removed after 8 weeks were fixed in 70% ethanol, dehydrated and embedded undecalcified in methyletacrylate (MMA). Sections (7.5 μm) were cut and stained with Goldner's trichrome. Care of animals was in accordance with institutional guidelines.

Periodic Acid-Schiff (PAS) reaction

Periodic acid primarily identifies glycogen in tissues by selectively oxidizing glucose residues, creating aldehydes that react with the Schiff reagent forming a magenta colour. Deparaffinised 4 μm thick sections of the tumors were rehydrated and stained with PAS reaction (Thies et al., 2001), omitting the Mayer's haemalum nuclear counterstain. The PAS-positive pattern, highlighted under a green filter, was evaluated under light microscopy using x100 magnification. Whole sections were screened for PAS-positive

Table 1. Phenotypic analysis of tumors formed after subcutaneous implantation of late passage hMSC–TERT20 cells or its subclones*.

Antigen	Antibody clone	Manufacturer	Dilution	#1#2#8	#3	#4	#5	#6#7	#9	#10	BB3 BC8 CE8	BD6 DB9	BD11
ASMA	1A4	Dako	1:200	+	-	-	+	+	+	+	-	-	+++
Calponin	CALP	Dako	1:1000	-	-	-	-	-	+++	+	ND	ND	ND
Desmin	DE-R-11	Dako	1:25	-	-	-	-	-	-	-	-	-	-
Myogenin	F5D	Dako	1:200	-	-	-	-	-	-	-	-	-	-
Biglycan	LF-112	NIDCR NIH	1:500	+++	+	+++	+	+	+	+	+++	+++	+++
Osteonectin	15G12	Novocastra	1:100	+++	+++	+++	+++	+++	+++	+++	+++	+++	+++
BSP	LF-83	NIDCR NIH	1:500	+++	+++	+++	+++	+++	+++	+++	+++	+++	+++
PINP	Rabbit Poly	Oulu Univ	1:400	+++	+++	+++	+++	+++	+++	+++	+++	+++	+++
Col Iα	LF-67	NIDCR NIH	1:1000	+++	+++	+++	+++	+++	+++	+++	+++	+++	+++
S-100	Z0311	Dako	1:8000	-	-	-	-	-	-	-	-	-	-
CD56	123C3	Monosan	1:50	-	-	-	-	-	-	-	-	-	-
CD31	JC/70A	Dako	1:50	-	-	-	-	-	-	-	-	-	-
CD34	QB-END10	Novocastra Lab	1:20	-	-	-	-	-	-	-	-	-	-
CD45	2B11+PD7	Dako	1:200	-	-	-	-	-	-	-	-	-	-
Laminin	Rabbit Poly	Sigma	1:100	+++	+++	+++	+++	+++	+++	+++	+++	+++	+++
Col IV	AB748	Chemicon	1:5000	+++	+++	+++	+++	+++	+++	+++	+++	+	+++
Cytokeratin	CAM5.2	BD PharMingen	1:20	-	-	-	-	-	-	-	-	-	-
EGFR	EGFR.113	Novocastra Lab	1:50	+++	+++	+++	+++	+++	+++	+++	+++	+++	+++
CD44	DF1485	Dako	1:200	+++	+++	+++	+++	+++	+++	+++	+++	+++	+++
CD99	12E7	Dako	1:100	+++	+++	+++	+++	+++	+++	+++	+++	+++	+++
Vimentin	V9	Dako	1:400	+++	+++	+++	+++	+++	+++	+++	+++	+++	+++

*: Indivdual hMSC-TERT20 tumors are labeled #1 to #10; subclones are denoted by suffix only.

extracellular matrix patterns within the tumor.

Microvessel staining and quantification

A 25-dot Chalkley microscope eyepiece graticule (West et al., 2005) was used as recommended by the international consensus on the quantification of angiogenesis (Vermeulen et al., 2002). This measured the relative area the vessels covered, correlating to the vessel number and microvessel density (MVD). Vessels were characterised by murine-specific CD34 immunocytochemistry using a rat monoclonal antibody (Clone MEC14.7 Abcam) and diaminobenzidine (DAB) as chromogen. Tissue counterstained for 2 min with Mayer's haematoxylin, was dehydrated and counted. Three independent tumors generated by the parental hMSC-TERT20 population or its clones were scanned at x40-100 magnification for areas with the highest microvessel density (hot spot). At x200 magnification, the Chalkley eyepiece graticule was orientated to each hot spot-area so that the maximum number of dots coincided with most vessel profiles. The mean of three separate counts provided the final Chalkley score within the area of 0.196 mm^2. Single observer counts were done without prior knowledge of the sample identity. Data concerning MVD was statistically compared using Mann-Whitney and Kruskall-Wallis tests.

Results

Cultured hMSC-TERT20 cells retained a normal SKY karyotype

Ex vivo expanded hMSC-TERT20 cells and clones shared monolayer morphologies, consisting of predominantly polygonal cells mixed with fusiform cells (Fig. 1A-G), forming a dense multilayered cobblestone pattern when confluent (Abdallah et al., 2005). FACS analysis indicated all clones had diploid DNA content (Fig. 1A-G), contrasting with the tetraploid control HT-1080 cell line (Fig. 1H). Despite continuous culture for three years, representing over 450 population doublings, G-banding (n=25) and SKY (n=10) indicated that the 46XY karyotype of hMSC-TERT20 cells was normal (Fig. 2).

Prognostic biomarker changes in cultured hMSC-TERT20 cells persist in tumors

Between PDL 116 and 442 the hMSC-TERT20 strain had a consistent population doubling time (average 1.3 days) (Fig. 3A). Unlike primary hMSC, immunocytochemistry showed that hMSC-TERT20 cells did not express the p16INK4a tumor suppressor protein, (Fig. 3B-D) confirming at the protein level a micro-deletion at the Ink4a/ARF exon 2 locus (Serakinci et al., 2004). Covert changes leading to tumorigenicity at PDL 256, did not alter *ex vivo* growth rate. Late passage hMSC-TERT20 cells showed increased expression of both Cyclin D1 (Fig. 3E-G) and p21Cip1/WAF1 (Fig. 3H-J). The cyclin dependent kinase inhibitor p27Kip1 was present in ≈ 72% of PDL 116 cells, but in only about 30% of the PDL 442 cells (Fig. 3K-M). Notably, even without p16 protein expression, the cells were capable of bone formation *in vivo* (Fig. 3N-P). The p53 staining intensity was greater in cultured hMSC-TERT20 cells (clearly detected in about 30% nuclei) versus the tumor cells (less than 5% positive nuclei). The hMSC-TERT20 tumours and its derived clones all retained nuclear expression of the mis-match repair proteins MLH1, MSH2 and MSH6, but the nuclei were negative for FLI-1 and NKX2.2 (Table 2).

Tumors sharing mesenchymal and osteogenic markers differed in alpha smooth muscle actin expression

Histomorphologically, tumors from clones hMSC-TERT20-BB3, -BD6, -CE8 and DB9 had densely packed

Table 2. Prognostic marker expression in early versus late passages of cultured hMSC-TERT20 cells and hMSC-TERT20 tumors*.

Antigen	Antibody clone	Manufacturer	Dilution	hMSC-TERT20 PDL 116	hMSC-TERT20 PDL 442	#1#2#5 #6#8#9	#3#4	#7	#10
ASMA	1A4	Dako	1:200	+++	+	+	-	+	+
CD99	12E7	Dako	1:100	+++	+	+++	+++	+++	+++
Cyclin D1	P2D11F11	NCL	1:200	+	+++	+++	+++	+++	+
$P16^{INK4a}$	E6H4	Dako	1:25	-	-	-	-	-	-
$P21^{WAF1/Cip1}$	EA10	Calbiochem	1:25	+	+++	+++	+++	+	+
$P27^{Kip1}$	57	Transduction Lab	1:100	+	+	+	+	+	+++
P53	DO7	Dako	1:100	+	+	-	-	-	-
pRB	G3-245	BD PharMingen	1:100	+++	+++	+++	+++	+++	+++
PMS2	A16-4	BD PharMingen	1:400	+++	+++	+++	+++	+++	+++
MLH1	G168-15	BD PharMingen	1:200	+++	+++	+++	+++	+++	+++
MSH2	27	Transduction Lab	1:800	+++	+++	+++	+++	+++	+++
MSH6	GTBP44	Serotec	1:400	+++	+++	+++	+++	+++	+++
FLI-1	polyclonal	Santa Cruz	1:300	-	-	-	-	-	-
NKX2.2	74.585	Hybridoma Bank	1:50	-	-	-	-	-	-

*: Indivdual hMSC-TERT20 tumors are labeled #1 to #10.

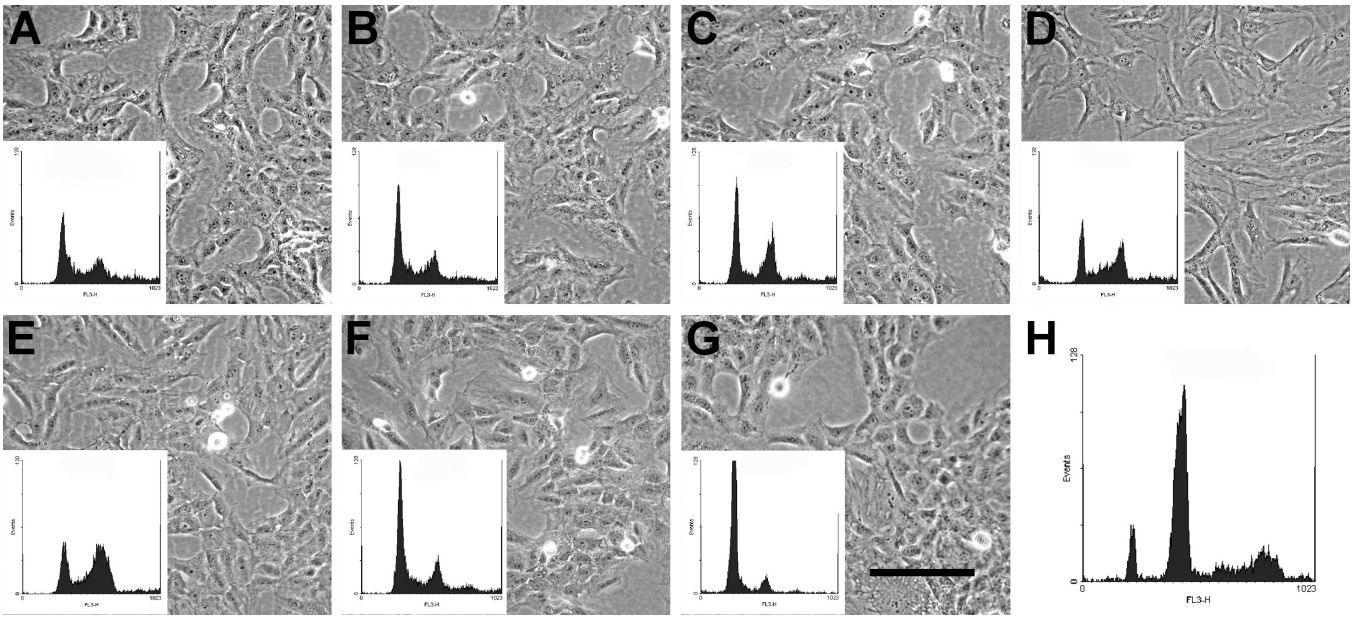

Fig. 1. Morphology of cultured clones and analysis of cell cycle. Phase-contrast photomicrographs. **A.** Clone hMSC-TERT20-BB3. **B.** Clone hMSC-TERT20-BC8. **C.** Clone hMSC-TERT20-BD6. **D.** Clone hMSC-TERT20-BD11. **E.** Clone hMSC-TERT20-CE8. **F.** Clone hMSC-TERT20-DB9. **G.** Strain hMSC-TERT20. **A-G. Inset.** FACS profile for propidium iodide labeling of DNA content. **H.** FACS profile for DNA content in tetraploid control cell line HT-1080. Bar: 100 μm.

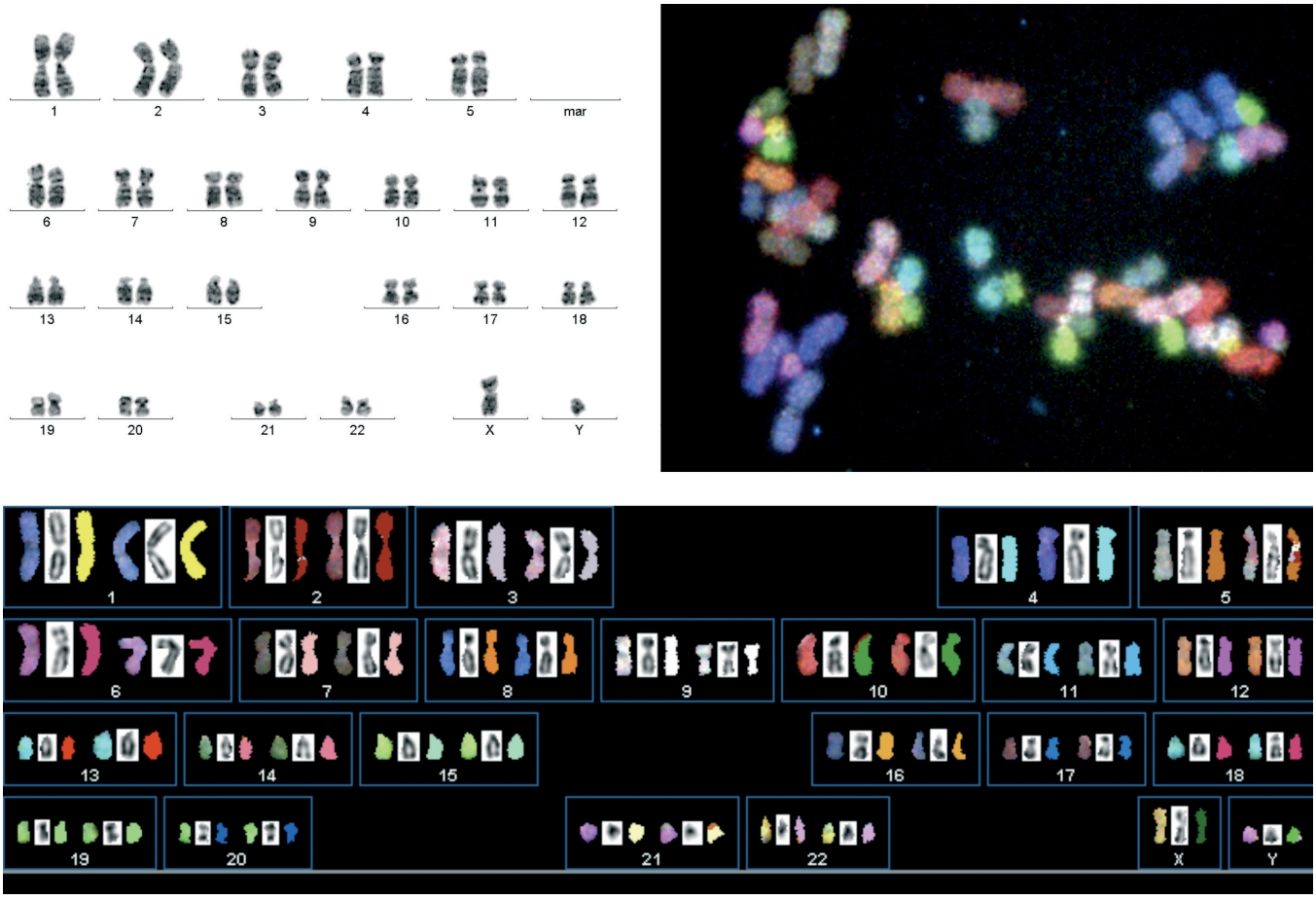

Fig. 2. Karyotypic analysis. Representative SKY and G-banding karyotype image from a metaphase spread of PDL 454 hMSC-TERT20 cells. A normal 46XY karyotype by G-banding (n=25) and spectral karyotyping (n=9) was obtained in every case. Any small discrepancies in SKY staining were not consistently observed and were attributable to overlapping chromosomes in the metaphase spread.

cuboidal cells, little cytoplasm, round nuclei and evenly distributed chromatin with inconspicuous nucleoli (Fig. 4). Biomarkers of mesenchymal cells; vimentin and EGFR were detectable in >90% of cells in all tumors (Table 1). Bone tissue biomarkers; the amino-terminal propeptide of type I procollagen (PINP), collagen type I alpha, osteonectin, bone sialoprotein, CD44 and biglycan were also strongly expressed. Notably, hMSC-TERT20 and clone-derived tumors strongly expressed the transmembrane glycoprotein CD99 (Fig. 5A) and the basal lamina proteins collagen IV and laminin.

Focal distribution of smooth muscle cell marker ASMA was found in eight out of ten tumors derived from the parental strain hMSC-TERT20 (Fig. 5B), but

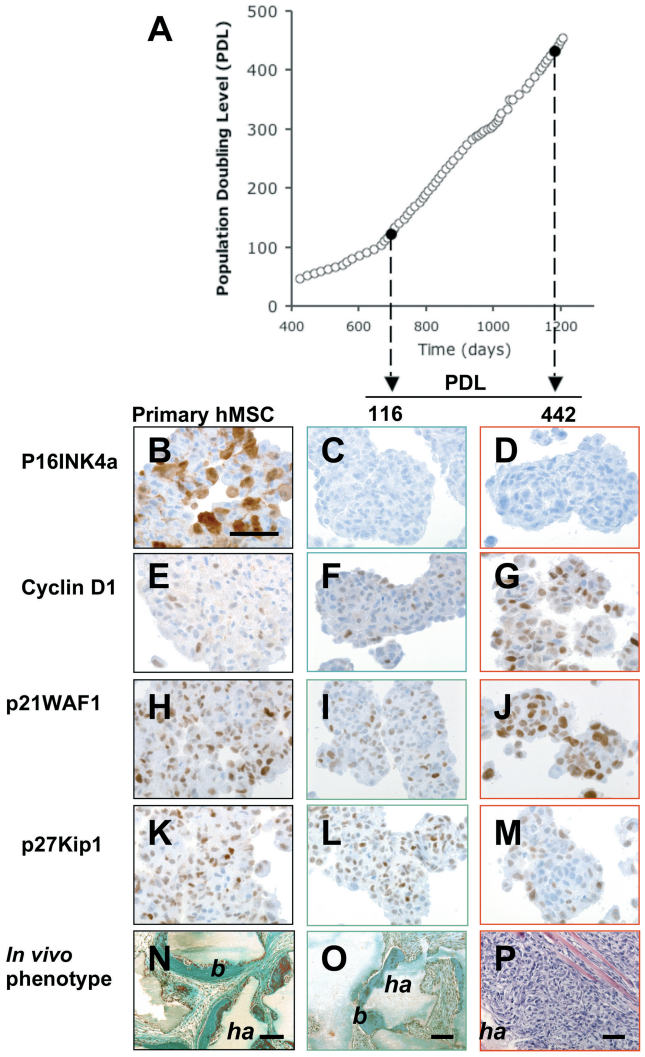

Fig. 3. Phenotypic changes during ex vivo expansion. **A.** Growth curve for hTERT transduced human mesenchymal cells continuously passaged at 1:20 (strain hMSC-TERT20). Days in culture refer to the cumulative period since infection with the hTERT retroviral vector. Population doubling levels (PDL) chosen for phenotypic analysis are indicated on the graph. **B-D.** Peroxidase immunocytochemical staining (brown) for $p16^{INK4a}$ in **(B)** Primary hMSC cells, **(C)** hMSC-TERT20 PDL116, **(D)** hMSC-TERT20 PDL 442. E-G, Staining for Cyclin D1 in **(E)** Primary hMSC cells, **(F)** hMSC-TERT20 PDL116, (G) hMSC-TERT20 PDL 442. **H-J.** Staining for p21WAF1/Cip1 in **(H)** Primary hMSC cells, **(I)** hMSC-TERT20 PDL116, **(J)** hMSC-TERT20 PDL 442. **K-M.** Staining for p27Kip1 in **(K)** Primary hMSC cells, **(L)** hMSC-TERT20 PDL116, **(M)** hMSC-TERT20 PDL 442. **N-P.** In vivo phenotype of xenografts implanted with hydroxyapatite tricalcium phosphate (ha) scaffold in immune compromised mice. **N.** Trichrome stain of primary hMSC cells after 8 weeks showing (b) bone osteoid deposition on the scaffold. **O.** Trichrome stain of hMSC-TERT20 PDL116 cells after 8 weeks. **P.** Haematoxylin and eosin stain of tumor derived from hMSC-TERT20 PDL 442. Bar: 100 μm.

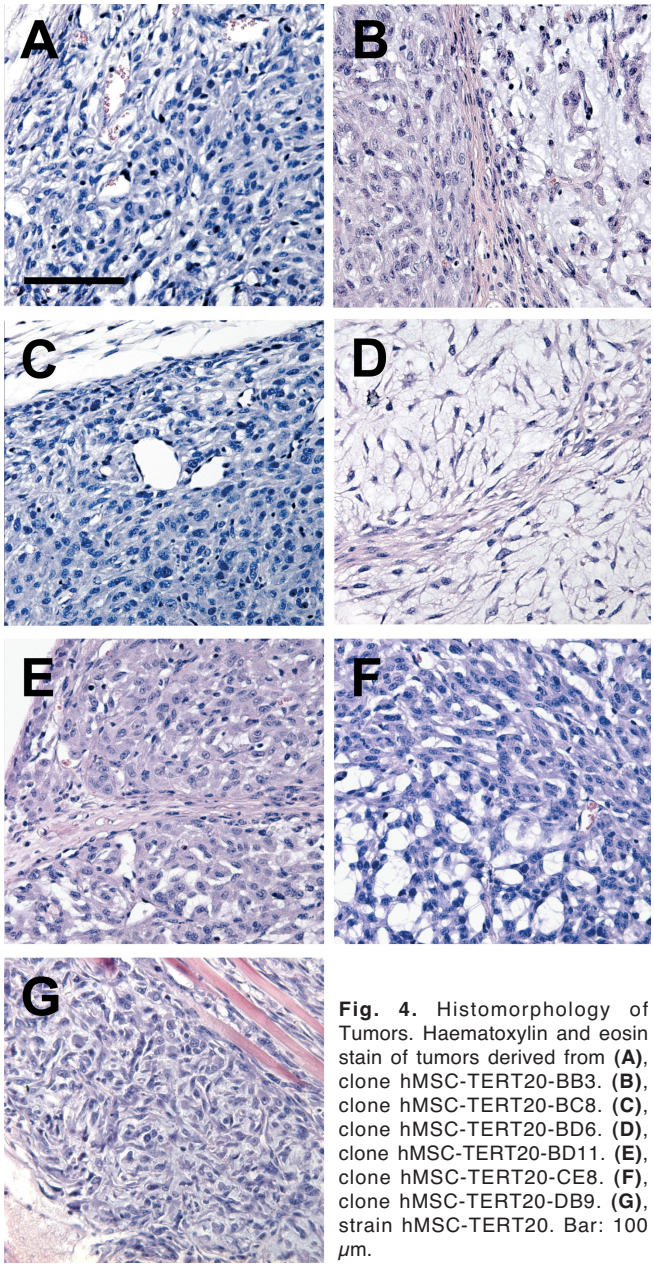

Fig. 4. Histomorphology of Tumors. Haematoxylin and eosin stain of tumors derived from **(A)**, clone hMSC-TERT20-BB3. **(B)**, clone hMSC-TERT20-BC8. **(C)**, clone hMSC-TERT20-BD6. **(D)**, clone hMSC-TERT20-BD11. **(E)**, clone hMSC-TERT20-CE8. **(F)**, clone hMSC-TERT20-DB9. **(G)**, strain hMSC-TERT20. Bar: 100 μm.

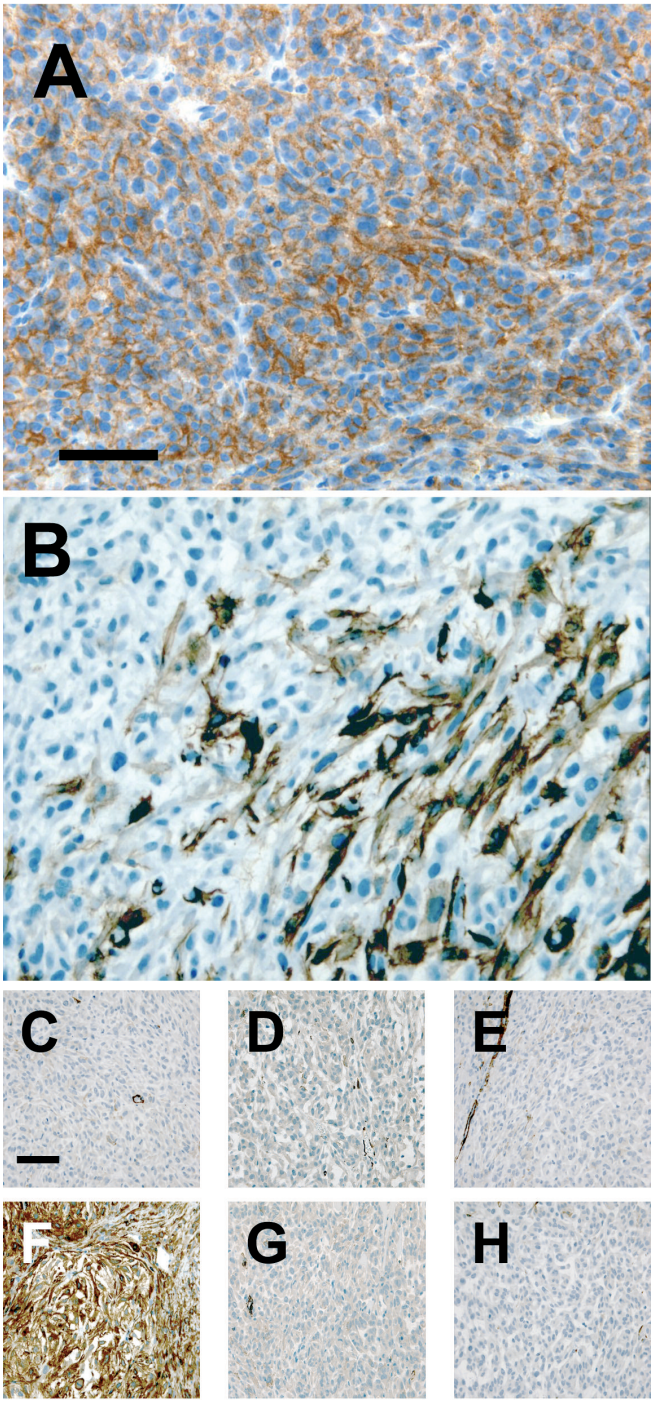

Fig. 5. CD99 expression and Alpha smooth muscle actin clonal heterogeneity. Peroxidase immunocytochemical staining (brown) in 4 μm sections of tumors derived from strain hMSC-TERT20 and its clones using the ARK method for **(A)** CD99 and **(B-H)** ASMA. **C.** Clone hMSC-TERT20-BB3. **D.** Clone hMSC-TERT20-BC8. **E.** Clone hMSC-TERT20-BD6. **F.** Clone hMSC-TERT20-BD11. **G.** Clone hMSC-TERT20-CE8. **H.** Clone hMSC-TERT20-DB9. Bar: 100 μm.

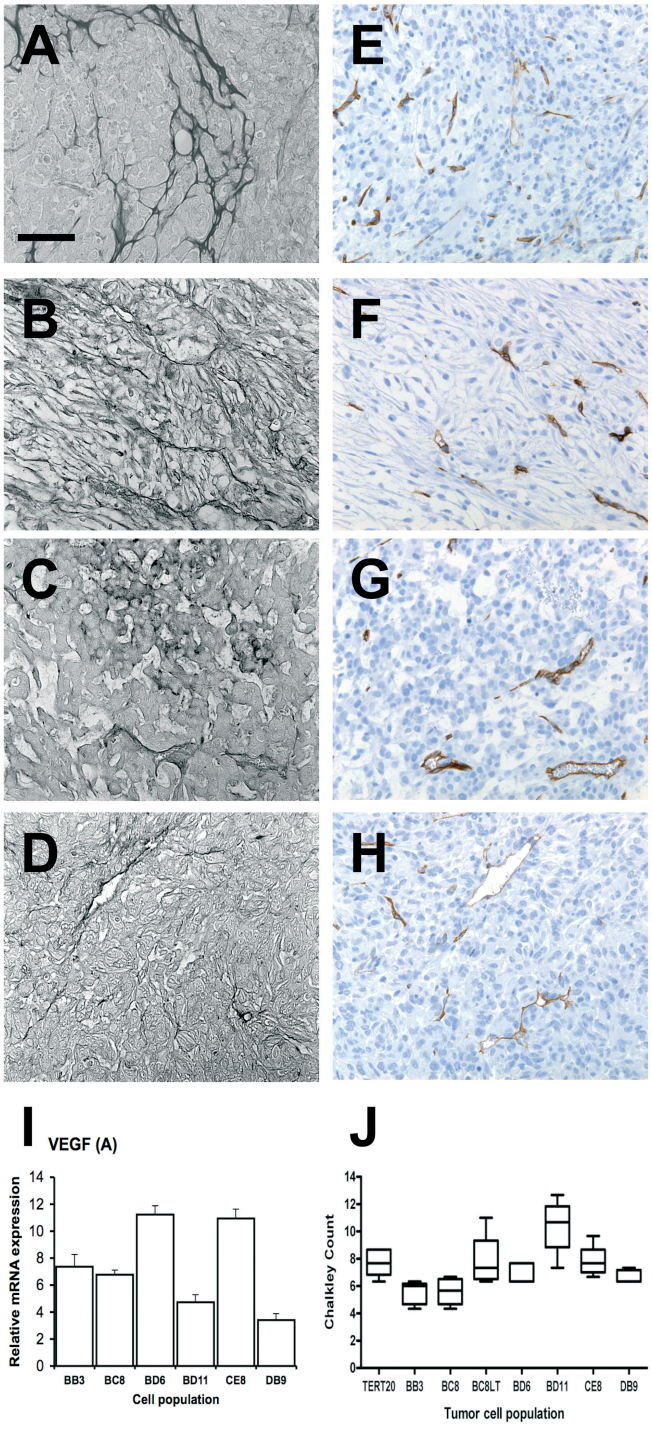

Fig. 6. Histological differences in tumor vasculature. **A-D.** Periodic acid-Schiff (PAS) staining (greyscale) of equivalent regions **(E-F)** with anti-CD34 immunohistochemical staining (brown) targeting murine endothelial cells in 4 μm sections of tumors derived from. **A, E.** Clone hMSC-TERT20-BC8. **B, F.** Clone hMSC-TERT20-BD11. **C, G.** Clone hMSC-TERT20-DB9. **D, H.** hMSC-TERT20-CE8. **I.** Real-time PCR analysis of relative mRNA expression of VEGF-A in the hMSC-TERT20 clones. Expression of target gene was normalized for ß-actin. Columns, mean of at least two independent experiments. **J.** Boxplot of mean Chalkley counts from five areas of three independent tumors originating from strain hMSC-TERT20 and six clones. Bar: 100 μm.

only tumors from clone hMSC-TERT20-BD11 expressed ASMA (Fig. 5C-H).

Clone-specific host vascular response

The pattern of periodic acid-Schiff (PAS) staining differed between the clones. hMSC-TERT20-BC8 had a subregion within a multi-lobed tumor with a strong looping PAS-positive looped pattern typical of that described for vasculogenic mimicry (Fig. 6A) (Lin et al., 2005). hMSC-TERT20-BD11 cells had a widely distributed PAS-positive cross-linked branching pattern around clusters of tumor cells. PAS staining was also observed in regions of the tumor section that did not stain for murine endothelial cells (Fig. 6B, F). hMSC-TERT20-BB3 and -DB9 tumors had a very different punctate pattern of PAS positive reaction in central regions of the tumor (Fig. 6C). In contrast, clone hMSC-TERT20-CE8 and -BD6 cells had a weaker PAS pattern that followed the host $CD34^+$ vasculature (Fig. 6D, H). RT-PCR analysis showed that all clones expressed the potently angiogenic vasculature endothelial growth factor (VEGF-A) (Fig. 6I), but relative mRNA levels did not directly correspond to tumor growth rate. In most cases, CD34 stained vessels were evenly distributed across the whole tumor section. hMSC-TERT20-BD11 tumor sections were distinguished by uneven blood vessel distribution, including some visual fields without blood vessels and others with angiogenic hot-spots having the highest mean Chalkley count of 11 ($p<0.0006$, Kruskal-Wallis) (Fig. 6J). The hMSC-TERT20-BC8 clone, characterized by a reduced tumorigenic potential (Burns et al., 2005), had the lowest mean Chalkley count of 5.6. An exceptional hMSC-TERT20-BC8 tumor, which had a latent period of 97 days before growing as rapidly as the other clones, had a more equivalent Chalkley count of 7.8 ($p<0.05$, Mann-Whitney).

Discussion

In this study, we used histological characterization of hMSC-TERT20 tumors to show that they have retained mesenchymal and osteogenic markers, whilst acquiring oncogenic changes relevant to human sarcomas with a histochemical and histomorphological resemblance to Ewing's sarcoma. Previous studies using multiple genes have generated a neoplastic phenotype in human cells (Kendall et al., 2005; Mizumoto et al., 2006). However, the tumorigenic changes in hMSC-TERT20 cells evolved spontaneously *ex vivo*, with the only exogenously introduced gene being telomerase. Thus, apart from high levels of ectopic telomerase, our sarcoma model avoids any bias from artificially high oncogene expression levels, typical of consecutively engineered situations. Primary hMSC transfected with the telomerase negative control vector did not expand in culture (Simonsen et al., 2002). The hMSC-TERT20 diploid and SKY normal karyotype contrasted markedly with the abnormal karyotypes described in all other reports of spontaneously tumorigenic human mesenchymal stem cells (Xu et al., 2004; Rubio et al., 2005).

Cells extensively passaged *ex vivo* could potentially gain many different genetic changes, so it is intriguing that hMSC-TERT20 tumors acquired phenotypic traits seen in clinical sarcomas, in particular Ewing's sarcoma. A "nurture" hypothesis may propose that the culture microenvironment, containing serum in the growth medium, might mimick a wound-like tumor microenvironment (Dvorak, 1986). Alternatively, a "nature" hypothesis may argue that such similarities reflect innate properties of the cell targeted for sarcoma formation. Growing the appropriate tumor target cell in a suitable microenvironment (Lee et al., 2006a) is important for studies that address the emerging tumor stem cell concept (Gibbs et al., 2005). Our model highlights that tumorigenic changes associated with sarcomas *in vivo* can also spontaneously evolve in telomerized hMSC *ex vivo* and maintenance of genetic stability by telomerase activation was not protective against the development of cancer.

The histomorphology of hMSC-TERT20 clone tumors resembled small round blue cell sarcomas. A key biomarker that is used to help distinguish subsets within this sarcoma family is CD99, a 32 kDa glycoprotein encoded by the *mic2* gene. A high incidence of strong CD99 expression occurs in vimentin immunoreactive Ewing's sarcoma and peripheral neuroectodermal tumors (84%) (Llombart-Bosch and Navarro, 2001). Nonetheless, CD99 expression has also been reported in CD45 immunoreactive lymphoblastic lymphomas, desmin immunoreactive rhabdomyosarcomas and in cytokeratin positive synovial sarcoma (Helman and Meltzer, 2003). Overall however, the CD99+, Vimentin+, CD45-, desmin-, cytokeratin- phenotype of hMSC-TERT20 tumors was most consistent with a Ewing's sarcoma profile. Our hMSC-TERT20 model shared numerous other characteristics with Ewing's sarcoma. Telomerase is expressed at high levels in Ewing's sarcomas and is a target of the *EWS/FLI-1* oncogenic translocation (Takahashi et al., 2003; Fuchs et al., 2004). This may explain the relatively high karyotypic stability of Ewing's sarcomas. The loss of the p16INK4a pathway is a commonly observed prognostic factor in Ewing sarcoma samples (30%) (Kovar et al., 1997; Wei et al., 2000; Deneen and Denny, 2001) and is a frequent event in other models of telomerase-immortalized human cells (Darbro et al., 2006). Cyclin D1 is another *EWS/FLI-1* target gene and its overexpression is more prevalent in Ewing sarcomas than rhabdomyosarcomas (Zhang et al., 2004). Low immunohistochemical levels of p27 protein expression correlated with poor Ewing sarcoma survival (Matsunobu et al., 2004). In a recent analysis of microsatellite instability in Ewing tumours, most (54 out of 59 samples) showed nuclear expression of MLH1, MSH2 and MSH6 (Alldinger et al., 2007).

James Ewing proposed a vascular differentiation potential of Ewing sarcoma cells (Ewing, 2006). Some Ewing cell lines can form vascular-like tubes *ex vivo* (van der Schaft et al., 2005) and tumor cells have been reported to express alpha smooth muscle actin (ASMA) (Castillero-Trejo et al., 2005) and collagen type IV, which in non-neoplastic tissue is normally found exclusively in the basement membrane of smooth muscle and endothelial cells of the vascular wall (Roessner et al., 1982). Similarly, hMSC-TERT20-BD11 cells were capable of capillary morphogenesis *ex vivo* (Burns et al., 2005) and these cells expressed ASMA and collagen type IV. Observations regarding vasculogenesis in Ewing's sarcomas note that the tumor cells produce the VEGF-A isoform $VEGF_{165}$, which attracted bone marrow derived $CD34^+$ endothelial progenitor cells to the vascular bed (Lee et al., 2006b). In broad agreement, our hMSC-TERT20 clones all expressed VEGF-A. Among diverse mechanisms, both angiogenesis and vasculogenesis are considered to play a role in the growth of Ewing's sarcoma *in vivo* (Bolontrade et al., 2002). Vasculogenic mimicry, detectable by a characteristic PAS staining pattern, might be triggered by reduced oxygen tension and hypoxia to form an alternative circulatory system, independent of regular angiogenesis and endothelial proliferation (van der Schaft et al., 2005). Clone hMSC-TERT20-BC8 had rare regions with PAS-positive loops typical of vasculogenic mimicry and formed tumors with the lowest vessel density determined by Chalkley count. In hMSC-TERT20-DB9 and -BB3 tumors, central regions of the tumor had a punctate non-vascular PAS staining pattern. In summary, oxygen tension is likely to influence the PAS staining, but we saw little evidence to suggest that the tumor cells directly mimic the function of a vessel. Rather, in hMSC-TERT20-BD11, the tumor cells may have contributed to a high Chalkley count by having a pericyte-like ASMA+ phenotype. The *in vivo* vascular heterogeneity observed in our human mesenchymal stem cell tumorigenic model shared complexities found in sarcomas, with implications for anti-angiogenic strategies, including those aimed at targeting pericytes (Ozerdem, 2006).

Therefore, using routine histological methods, we readily detected several characteristics that would catalogue our sarcomas as fitting a Ewing sarcoma profile. However, though one would anticipate being able to detect *EWS/FLI-1* translocation by karyotypic analysis (Martinez-Ramirez et al., 2003), we found no evidence for this translocation in hMSC-TERT20 cells, not even with more sensitive SKY methods. Over 90% of Ewing sarcomas have a specific translocation fusing the EWS gene on chromosome 22 to one of five members of the ETS gene family (*FLI-1*, *ERG*, *ETV1*, *E1AF* and *FEV*). The chimeric nuclear protein product binds to DNA with similar specificity but greater potency (May et al., 1993). Thus, it may seem counterintuitive to discuss Ewing sarcoma in a tumor model that lacks the critical genetic translocation that ordinarily defines the tumorigenic phenotype. Without evidence for a Ewing sarcoma translocation event in hMSC-TERT20 cells, nor associated expression of FLI-1 or the target gene product NKX2.2, the similarities we observed must presumably reflect innate properties of the target cell rather than EWS/FLI-1 driven events. Nonetheless, since the Ewing sarcoma translocation event is associated with activation of high levels of telomerase expression, our model remains very relevant in this aspect. It emphasizes that in the context of hMSC cells, telomerase would potentially be a very significant EWS/ETS target gene. Indeed, our hMSC model represents the first known example whereby ectopic expression of telomerase and long term *ex vivo* culture sufficed for the evolution of tumorigenesis in human cells.

Consistent with our conjecture, there is growing evidence that mesenchymal stromal cells (hMSC) residing in the bone marrow may be the cell origin of Ewing's sarcoma. *EWS/FLI-1* expression blocked the osteogenic differentiation of murine marrow stromal cells (Torchia et al., 2003). hMSC can mobilise to extraskeletal sites, possibly accounting for the rare Ewing sarcomas resembling those found in bone, but arising in almost any soft tissue (Delattre et al., 1994). Significantly, the EWS/FLI-1 fusion oncogene has cell context specific effects. Paradoxically, it has toxic or senescence-inducing effects in adult human fibroblasts (Lessnick et al., 2002) and in murine NIH3T3 cells failed to induce expression of NKX2.2 (Braunreiter et al., 2006), a target found to be required for the oncogenic phenotype of Ewing's sarcoma (Smith et al., 2006). In contrast, the *EWS/FLI-1* fusion oncogene generated Ewing's sarcoma-like tumors in primary murine bone marrow derived MSC (Castillero-Trejo et al., 2005; Riggi et al., 2005). In the latter study, the ability of MSC to host the EWS/FLI-1 oncogene was deemed strong evidence that they may be ontogenic candidates for Ewing's sarcoma. However, the ability of murine cells to express a CD99 homologue was debated (Kovar and Bernard, 2006), emphasizing that a human cell model would be preferred. More recently, Tirode et al., reasoned that since the ultimate phenotype of Ewing's tumor cells is likely to reflect both the cell lineage from which it is derived and specific effects of EWS/FLI-1, removing the latter might recover characteristics of the primary cell of origin. They successfully applied short hairpin RNA (shRNA) silencing of EWS/FLI-1 in human Ewing sarcoma cell lines. This also down regulated some neural crest genes not ordinarily found on hMSC. Furthermore, EWS/FLI-1 suppressed Ewing cells could express early differentiation biomarkers when induced towards adipocyte, osteoblast or chondrocyte lineages (Tirode et al., 2007). Thus, human Ewing sarcoma cell lines without expression of the EWS/FLI-1 fusion oncogene converged to a profile that resembled mesenchymal stem cells (MSC). Our model provides novel complementary evidence that bona fide hMSC expressing the EWS/FLI-1 target gene

telomerase, may spontaneously acquire a tumorigenic profile that indirectly resembles Ewing sarcomas.

We propose that hMSC would be an appropriate target cell for experiments that aim to provide more direct evidence by reconstructing the Ewing sarcoma phenotype with the EWS/ETS fusion oncogene. In addition, distinct phenotypes among the clones provide a model system to address specific questions concerning tumorigenesis and vascularisation. Such molecular analysis could also provide clues regarding desirable qualities when selecting adult mesenchymal stem cells for regenerative medicine to improve vasculature in ischaemic situations.

Note added in proof:

A recent study provides further compelling evidence that hMSC are likely to be the target cells for Ewing's sarcoma (Riggi et al., 2008).

Acknowledgements. This work was supported by the Danish Medical Research Council, Danish Center for Stem Cell Research, Karen Elise Jensen's Fond, Novo Nordisk Foundation, Gross M. Brogaard og Hustru Foundation, Jacob Madsen og Hustru Foundation and Danish Lægeforening Research Foundation.

References

Abdallah B.M., Haack-Sorensen M., Burns J.S., Elsnab B., Jakob F., Hokland P. and Kassem M. (2005). Maintenance of differentiation potential of human bone marrow mesenchymal stem cells immortalized by human telomerase reverse transcriptase gene despite [corrected] extensive proliferation. Biochem. Biophys. Res. Commun. 326, 527-538.

Alldinger I., Schaefer K.L., Goedde D., Ottaviano L., Dirksen U., Ranft A., Juergens H., Gabbert H.E., Knoefel W.T. and Poremba C. (2007). Microsatellite instability in Ewing tumor is not associated with loss of mismatch repair protein expression. J. Cancer Res. Clin. Oncol. 133, 749-759.

Bagley R.G., Weber W., Rouleau C. and Teicher B.A. (2005). Pericytes and endothelial precursor cells: cellular interactions and contributions to malignancy. Cancer Res. 65, 9741-9750.

Bjerkvig R., Tysnes B.B., Aboody K.S., Najbauer J. and Terzis A.J. (2005). Opinion: the origin of the cancer stem cell: current controversies and new insights. Nat. Rev. Cancer 5, 899-904.

Bolontrade M.F., Zhou R.R. and Kleinerman E.S. (2002). Vasculogenesis plays a role in the growth of ewing's sarcoma *in vivo*. Clin. Cancer Res. 8, 3622-3627.

Braunreiter C.L., Hancock J.D., Coffin C.M., Boucher K.M. and Lessnick S.L. (2006). Expression of EWS-ETS fusions in NIH3T3 cells reveals significant differences to Ewing's sarcoma. Cell Cycle 5, 2753-2759.

Burns J.S., Abdallah B.M., Guldberg P., Rygaard J., Schroder H.D. and Kassem M. (2005). Tumorigenic heterogeneity in cancer stem cells evolved from long-term cultures of telomerase-immortalized human mesenchymal stem cells. Cancer Res. 65, 3126-3135.

Castillero-Trejo Y., Eliazer S., Xiang L., Richardson J.A. and Ilaria R.L.J. (2005). Expression of the EWS/FLI-1 oncogene in murine primary bone-derived cells Results in EWS/FLI-1-dependent, ewing sarcoma-like tumors. Cancer Res. 65, 8698-8705.

Clark M.A., Fisher C., Judson I. and Thomas J.M. (2005). Soft-tissue sarcomas in adults. N. Engl. J. Med. 353, 701-711.

Crowe D.L., Parsa B. and Sinha U.K. (2004). Relationships between stem cells and cancer stem cells. Histol. Histopathol. 19, 505-509.

Darbro B.W., Lee K.M., Nguyen N.K., Domann F.E. and Klingelhutz A.J. (2006). Methylation of the p16(INK4a) promoter region in telomerase immortalized human keratinocytes co-cultured with feeder cells. Oncogene 25, 7421-7433.

Delattre O., Zucman J., Melot T., Garau X.S., Zucker J.M., Lenoir G.M., Ambros P.F., Sheer D., Turc-Carel C. and Triche T.J. (1994). The Ewing family of tumors--a subgroup of small-round-cell tumors defined by specific chimeric transcripts. N. Engl. J. Med. 331, 294-299.

Deneen B. and Denny C.T. (2001)Loss of p16 pathways stabilizes EWS/FLI1 expression and complements EWS/FLI1 mediated transformation. Oncogene 20, 6731-6741.

Dvorak H.F. (1986). Tumors: wounds that do not heal. Similarities between tumor stroma generation and wound healing. N. Engl. J. Med. 315, 1650-1659.

Ewing J. (2006). The Classic: Diffuse endothelioma of bone. Proceedings of the New York Pathological Society. 1921;12:17. Clin Orthop Relat Res 450, 25-27.

Folberg R. and Maniotis A.J. (2004). Vasculogenic mimicry. APMIS 112, 508-525.

Fuchs B., Inwards C., Scully S.P. and Janknecht R. (2004). hTERT Is highly expressed in Ewing's sarcoma and activated by EWS-ETS oncoproteins. Clin. Orthop. Relat. Res. 64-68.

Garcia-Barros M., Paris, F., Cordon-Cardo C., Lyden D., Rafii S., Haimovitz-Friedman A., Fuks Z. and Kolesnick R. (2003). Tumor response to radiotherapy regulated by endothelial cell apoptosis. Science 300, 1155-1159.

Gibbs C.P., Kukekov V.G., Reith J.D., Tchigrinova O., Suslov O.N., Scott E.W., Ghivizzani S.C., Ignatova T.N. and Steindler D.A. (2005). Stem-like cells in bone sarcomas: implications for tumorigenesis. Neoplasia 7, 967-976.

Grier H.E., Krailo M.D., Tarbell N.J., Link M.P., Fryer C.J., Pritchard D.J., Gebhardt M.C., Dickman P.S., Perlman E.J., Meyers P.A., Donaldson S.S., Moore S., Rausen A.R., Vietti T.J. and Miser J.S. (2003). Addition of ifosfamide and etoposide to standard chemotherapy for Ewing's sarcoma and primitive neuroectodermal tumor of bone. N. Engl J. Med. 348, 694-701.

Hansen M.F., Koufos A., Gallie B.L., Phillips R.A., Fodstad O., Brogger A., Gedde-Dahl T. and Cavenee W.K. (1985). Osteosarcoma and retinoblastoma: a shared chromosomal mechanism revealing recessive predisposition. Proc. Natl. Acad. Sci. USA 82, 6216-6220.

Helman L.J. and Meltzer P. (2003). Mechanisms of sarcoma development. Nat. Rev. Cancer 3, 685-694.

Kendall S.D., Linardic C.M., Adam S.J. and Counter C.M. (2005). A network of genetic events sufficient to convert normal human cells to a tumorigenic state. Cancer Res. 65, 9824-9828.

Kinnaird T., Stabile E., Burnett M.S. and Epstein S.E. (2004). Bone-marrow-derived cells for enhancing collateral development: mechanisms, animal data, and initial clinical experiences. Circ. Res. 95, 354-363.

Kovar H. and Bernard A. (2006). CD99-positive "Ewing's sarcoma" from mouse-bone marrow-derived mesenchymal progenitor cells? Cancer Res. 66, 9786; author reply 9786.

Kovar H., Jug G., Aryee D.N., Zoubek A., Ambros P., Gruber B.,

Windhager R. and Gadner H. (1997). Among genes involved in the RB dependent cell cycle regulatory cascade, the p16 tumor suppressor gene is frequently lost in the Ewing family of tumors. Oncogene 15, 2225-2232.

Lee J., Kotliarova S., Kotliarov Y., Li A., Su Q., Donin N.M., Pastorino S., Purow B.W., Christopher N., Zhang W., Park J.K. and Fine H.A. (2006a). Tumor stem cells derived from glioblastomas cultured in bFGF and EGF more closely mirror the phenotype and genotype of primary tumors than do serum-cultured cell lines. Cancer Cell 9, 391-403.

Lee T.H., Bolontrade M.F., Worth L.L., Guan H., Ellis L.M. and Kleinerman E.S. (2006b). Production of VEGF165 by Ewing's sarcoma cells induces vasculogenesis and the incorporation of CD34+ stem cells into the expanding tumor vasculature. Int. J. Cancer 119, 839-846.

Lessnick S.L., Dacwag C.S. and Golub T.R. (2002). The Ewing's sarcoma oncoprotein EWS/FLI induces a p53-dependent growth arrest in primary human fibroblasts. Cancer Cell 1, 393-401.

Lin A.Y., Maniotis A.J., Valyi-Nagy K., Majumdar D., Setty S., Kadkol S., Leach L., Pe'er J. and Folberg R. (2005). Distinguishing fibrovascular septa from vasculogenic mimicry patterns. Arch. Pathol. Lab. Med. 129, 884-892.

Llombart-Bosch A. and Navarro S. (2001). Immunohistochemical detection of EWS and FLI-1 proteinss in Ewing sarcoma and primitive neuroectodermal tumors: comparative analysis with CD99 (MIC-2) expression. Appl. Immunohistochem. Mol. Morphol. 9, 255-260.

Martinez-Ramirez A., Rodriguez-Perales S., Melendez B., Martinez-Delgado B., Urioste M., Cigudosa J.C. and Benitez J. (2003). Characterization of the A673 cell line (Ewing tumor) by molecular cytogenetic techniques. Cancer Genet. Cytogenet. 141, 138-142.

Matsunobu T., Tanaka K., Matsumoto Y., Nakatani F., Sakimura R., Hanada M., Li X., Oda Y., Naruse I., Hoshino H., Tsuneyoshi M., Miura H. and Iwamoto Y. (2004). The prognostic and therapeutic relevance of p27kip1 in Ewing's family tumors. Clin. Cancer Res. 10, 1003-1012.

May W.A., Lessnick S.L., Braun B.S., Klemsz M., Lewis B.C., Lunsford L.B., Hromas R. and Denny C.T. (1993). The Ewing's sarcoma EWS/FLI-1 fusion gene encodes a more potent transcriptional activator and is a more powerful transforming gene than FLI-1. Mol. Cell Biol. 13, 7393-7398.

Mizumoto Y., Kyo S., Ohno S., Hashimoto M., Nakamura M., Maida Y., Sakaguchi J., Takakura M., Inoue M. and Kiyono T. (2006). Creation of tumorigenic human endometrial epithelial cells with intact chromosomes by introducing defined genetic elements. Oncogene 25, 5673-5682.

Ozerdem U. (2006). Targeting pericytes diminishes neovascularization in orthotopic uveal melanoma in nerve/glial antigen 2 proteoglycan knockout mouse. Ophthalmic Res. 38, 251-254.

Riggi N., Cironi L., Provero P., Suva M. L., Kaloulis K., Garcia-Echeverria C., Hoffmann F., Trumpp A. and Stamenkovic I. (2005). Development of Ewing's sarcoma from primary bone marrow-derived mesenchymal progenitor cells. Cancer Res. 65, 11459-11468.

Riggi N., Suva M.-L., Suva D., Cironi L., Provero P., Tercier S., Joseph J.-M., Stehle J.-C., Baumer K., Kindler V. and Stamenovic I., (2008). EWS-FLI-1 expression triggers a Ewing's sarcoma initiation program in primary human mesenchymal stem cells. Cancer Res. 68, 2176-2185.

Roessner A., Voss B., Rauterberg J., Immenkamp M., and Grundmann E. (1982). Biologic characterization of human bone tumors. I. Ewing's sarcoma. A comparative electron and immunofluorescence microscopic study. J. Cancer Res. Clin. Oncol. 104, 171-180.

Rubio D., Garcia-Castro J., Martin M.C., de la Fuente R., Cigudosa J.C., Lloyd A.C. and Bernad A. (2005). Spontaneous human adult stem cell transformation. Cancer Res. 65, 3035-3039.

Schrock E., Veldman T., Padilla-Nash H., Ning Y., Spurbeck J., Jalal S., Shaffer L.G., Papenhausen P., Kozma C., Phelan M.C., Kjeldsen E., Schonberg S.A., O'Brien P., Biesecker L., du Manoir S. and Ried T. (1997). Spectral karyotyping refines cytogenetic diagnostics of constitutional chromosomal abnormalities. Hum. Genet. 101, 255-262.

Serakinci N., Guldberg P., Burns J.S., Abdallah B., Schrodder H., Jensen T. and Kassem M. (2004). Adult human mesenchymal stem cell as a target for neoplastic transformation. Oncogene 23, 5095-5098.

Simonsen J.L., Rosada C., Serakinci N., Justesen J., Stenderup K., Rattan S.I., Jensen T.G. and Kassem M. (2002). Telomerase expression extends the proliferative life-span and maintains the osteogenic potential of human bone marrow stromal cells. Nat. Biotechnol. 20, 592-596.

Smith R., Owen L.A., Trem D.J., Wong J.S., Whangbo J.S., Golub T.R. and Lessnick S.L. (2006). Expression profiling of EWS/FLI identifies NKX2.2 as a critical target gene in Ewing's sarcoma. Cancer Cell 9, 405-416.

Takahashi A., Higashino F., Aoyagi M., Yoshida K., Itoh M., Kyo S., Ohno T., Taira T., Ariga H., Nakajima K., Hatta M., Kobayashi M., Sano H., Kohgo T. and Shindoh M. (2003). EWS/ETS fusions activate telomerase in Ewing's tumors. Cancer Res. 63, 8338-8344.

Thies A., Mangold U., Moll I. and Schumacher U. (2001). PAS-positive loops and networks as a prognostic indicator in cutaneous malignant melanoma. J. Pathol. 195, 537-542.

Tirode F., Laud-Duval K., Prieur A., Delorme B., Charbord P. and Delattre O. (2007). Mesenchymal stem cell features of Ewing tumors. Cancer Cell 11, 421-429.

Torchia E.C., Jaishankar S. and Baker S.J. (2003). Ewing tumor fusion proteins block the differentiation of pluripotent marrow stromal cells. Cancer Res. 63 3464-3468.

van der Schaft D.W. Hillen F., Pauwels P., Kirschmann D.A., Castermans K., Egbrink M.G. Tran M.G. Sciot R. Hauben E., Hogendoorn P.C. Delattre O., Maxwell P.H., Hendrix M.J. and Griffioen A.W. (2005). Tumor cell plasticity in Ewing sarcoma, an alternative circulatory system stimulated by hypoxia. Cancer Res. 65, 11520-11528.

Vermeulen P.B., Gasparini G., Fox S.B., Colpaert C., Marson L.P., Gion M., Belien J.A., de Waal R.M., Van Marck E., Magnani E., Weidner N., Harris A.L. and Dirix LY. (2002). Second international consensus on the methodology and criteria of evaluation of angiogenesis quantification in solid human tumours. Eur. J. Cancer 38, 1564-1579.

Wei G., Antonescu C.R., de Alava E., Leung D., Huvos A.G., Meyers P. A., Healey J.H. and Ladanyi M. (2000). Prognostic impact of INK4A deletion in Ewing sarcoma. Cancer 89, 793-799.

Weitz J., Antonescu C.R. and Brennan M.F. (2003). Localized extremity soft tissue sarcoma: improved knowledge with unchanged survival over time. J. Clin. Oncol. 21, 2719-2725.

West C.C., Brown N.J., Mangham D.C., Grimer R.J., and Reed M.W. (2005). Microvessel density does not predict outcome in high grade

soft tissue sarcoma. Eur. J. Surg. Oncol. 31, 1198-1205.

Xu W., Qian H., Zhu W., Chen Y., Shao Q., Sun X., Hu J., Han C. and Zhang X. (2004). A novel tumor cell line cloned from mutated human embryonic bone marrow mesenchymal stem cells. Oncol. Rep. 12, 501-508.

Yunis J.J. (1976). High resolution of human chromosomes. Science 191, 1268-1270.

Zhang J., Hu S., Schofield D.E., Sorensen P.H. and Triche T.J. (2004). Selective usage of D-Type cyclins by Ewing's tumors and rhabdomyosarcomas. Cancer Res. 64, 6026-6034.

Accepted April 25, 2008